Power-law decay of homogeneous turbulence at low Reynolds numbers

Mei-Jiau Huang
Division of Engineering and Applied Science, California Institute of Technology, Pasadena, California 91125

Anthony Leonard
Graduate Aeronautical Laboratories, California Institute of Technology, Pasadena, California 91125

(Received 27 January 1994; accepted 11 July 1994)

The decay of nominally isotropic, homogeneous incompressible turbulence is studied by direct numerical simulations for Re_λ in the range (5–50) with 256^3 spectral coefficients. A power-law decay of the turbulent energy is observed with exponents approximately equal to 1.5 and 1.25, apparently dependent on Re_λ. A new complete similarity form for the double and triple velocity correlation functions, $f(r,t)$ and $k(r,t)$, is proposed for low to intermediate Re_λ that is consistent with the Kármán–Howarth equation and the results of the numerical experiments. The results are also consistent with Saffman's proposed asymptotic behavior of $f(r,t)$ for large separation r for runs with a decay exponent of 1.5. The so-called final period of decay is not observed.

I. INTRODUCTION

Grid-generated turbulence was first extensively studied by Batchelor and Townsend.[1–3] The turbulence, which was nearly isotropic and homogeneous, was observed to have a power-law decay in energy. They distinguished three stages of the decay: an initial period, during which turbulence is being developed, a transition period, and a final period, during which viscous forces are believed to dominate inertial forces throughout the full wave-number range. The associated decay exponent was found to be about one for the initial period of decay and 2.5 for the final period. More recent measurements made by Sato and Yamamoto[4] also followed a power-law decay with exponent 2.5 in the final period, but found exponents between 1 and 1.3 for the initial period of decay. Recently, Smith *et al.*[5] measured the decay of enstrophy for towed grid-generated turbulence with grid Reynolds number of order 10^5 without using Taylor's "frozen field" hypothesis. They observed a power-law decay of the root-mean-square (RMS) vorticity with an exponent of 1.5 ± 0.2, corresponding to a decay exponent of 2 for the turbulent energy.

Results of numerical simulations of turbulence at small Reynolds numbers were studied by Mansour and Wray.[6] Power-law decays were observed and decay exponents between 1.1 and 2.5 were found depending on the Reynolds number and on the behavior of the energy spectrum at low wave numbers. The decay exponent 1.5 for the RMS vorticity was observed in numerical experiments by Herring and Kerr,[7] also.

On the theoretical side, a number of analyses, based on various assumptions, have been developed to treat decaying homogeneous turbulence. As an example, one may start with the hypothesis of complete and/or partial self-similarity of the double and triple velocity correlation functions and use the Kármán–Howarth equation[8] to deduce further results. A detailed study of self-similar solutions of the Kármán–Howarth equation and their stable equilibria can be found in Speziale and Bernard[9] (also see Batchelor[10]). They conclude that completely self-similar solutions always lead to a decay exponent of one, unless the Reynolds number is zero, a state that can be reached only as time goes to infinity.

Partially self-similar solutions, i.e., correlation functions that are self-similar only for some ranges of r, can lead to decay exponents other than one. Some of the criteria required by complete self-similarity must be relaxed and replaced by other assumptions. For example, by relaxing the criterion that the scaling length has to be Taylor's microscale, a decay exponent of 10/7 can be obtained provided Loitsianskii's integral is invariant in time[11] while, on the other hand, an exponent of 6/5 is found if Saffman's invariant is assumed.[12]

To predict the power-law decay during the final period, one ignores the inertial force in the energy equation (almost by definition of "final period"). The turbulent energy can then be determined by

$$K\sim\int_0^\infty E(k,t_o)\exp[-2\nu k^2(t-t_o)]dk, \tag{1}$$

where $E(k,t)$ is the three dimensional energy spectrum, k is the magnitude of the wave vector $\mathbf{k}$ and t_o is some reference time. Because of the exponential factor in the integrand, contributions from small wave numbers dominate and a power-law behavior of $E(k,t_o)$ near $k=0$ results in a power-law decay of turbulent energy. A decay exponent of 2.5, therefore, follows from an analytic behavior of $E_{ij}(k,t_o)$, the energy spectral tensor, near the origin,[13] namely,

$$E(k)\sim C_2k^4+o(k^4). \tag{2}$$

However, Batchelor and Proudman[14] studied the asymptotic form for large separations of the double and triple velocity correlations based on their hypothesis and obtained a nonanalytic behavior of the energy spectral tensor near the origin. Saffman[12] subsequently modified the hypothesis and made it less restrictive. He showed, in general, that the

 1070-6631/94/6(11)/3765/11/$6.00

double correlation function is $\mathcal{O}(r^{-3})$ for large separation. This corresponds to a nonanalytic behavior of energy spectra near the origin with the result

$$E(k)\sim C_0k^2+o(k^2). \tag{3}$$

The decay exponent then becomes 1.5 for the final period of decay.

In this paper we study the decay problem by numerically simulating incompressible homogeneous turbulence. Decay exponents are found and a new self-similarity is proposed that is consistent with the numerical results and the Kármán–Howarth equation. The paper is arranged as follows. In Sec. II we give a short review of the classical similarity theories mentioned above and propose a new similarity form for the velocity correlation functions. Numerical techniques and results are presented in Sec. III. Summary and conclusions are given in Sec. IV.

II. THEORETICAL BACKGROUND

A. Previous similarity hypotheses

We investigate the energy decay of incompressible turbulent flow which is governed by the Navier–Stokes equations

$$\frac{\partial \mathbf{u}}{\partial t}+\mathbf{u}\cdot\nabla\mathbf{u}=-\nabla p+\nu\nabla^2\mathbf{u}, \tag{4a}$$

$$\nabla\cdot\mathbf{u}=0, \tag{4b}$$

where $\mathbf{u}$ is the turbulent velocity, p is the pressure, and ν is the kinematic viscosity. In this paper, we restrict our attention to isotropic homogeneous turbulence. Because of homogeneity, isotropy, and the incompressibility, the two-point second-order moment tensors of velocity can be expressed in term of a single scalar function $f(r,t)$, the longitudinal velocity correlation coefficient, defined as

$$f(r,t)\equiv\overline{u(\mathbf{x},t)u(\mathbf{x}+\mathbf{r},t)}/q(t)^2, \tag{5}$$

where r is the separation of the two points, t is the time, u is the velocity component in the $\mathbf{r}$ direction, and $\frac{3}{2}q^2$ is the turbulent energy. Similarly, $k(r,t)$, the triple velocity correlation coefficient, is defined as

$$k(r,t)\equiv\overline{u(\mathbf{x},t)^2u(\mathbf{x}+\mathbf{r},t)}/q(t)^3. \tag{6}$$

The dynamical equation connecting these two scalar functions derived by Kármán and Howarth[8] from the Navier–Stokes equations is given by

$$\frac{\partial(q^2f)}{\partial t}=q^3\left(\frac{\partial k}{\partial r}+\frac{4}{r}k\right)+2\nu q^2\left(\frac{\partial^2 f}{\partial r^2}+\frac{4}{r}\frac{\partial f}{\partial r}\right). \tag{7}$$

Kármán and Howarth[8] showed that completely self-similar solutions of the above equation, if they exist, must be of the form

$$f(r,t)=\tilde{f}[r/\lambda(t)] \quad \text{and} \quad k(r,t)=\tilde{k}[r/\lambda(t)] \tag{8a}$$

and two constraints,

$$q\cdot\lambda=\text{const} \tag{8b}$$

and

$$\lambda\frac{d\lambda}{dt}=\text{const}, \tag{8c}$$

must be satisfied. Here λ is the Taylor microscale[8,9,13] defined by

$$\lambda^2\equiv\frac{5\int_0^\infty E(k)dk}{\int_0^\infty k^2E(k)dk}. \tag{9}$$

A power-law decay of the turbulent energy is consequently obtained with the decay exponent equal to one, that is,

$$K\equiv\tfrac{3}{2}q^2\sim t^{-1}. \tag{10}$$

Although early experiments[2,15,16] seemed consistent with this power-law decay, a subsequent study by Comte-Bellot and Corrsin[17] shows even a better fit to their experimental data with decay exponents in the range, approximately, from 1.1 to 1.4 by adding a virtual time origin to the fit.

A more general hypothesis of similarity may be formulated such that the decay exponent $\neq 1$. George,[18] instead of assigning a self-similarity of the correlation coefficients, assumed a self-similar energy spectrum, $E(k,t)$ and energy transfer spectrum, $T(k,t)$, as follows:

$$E(k,t)=E_s(t)\tilde{E}(k\mathscr{L}), \tag{11a}$$

$$T(k,t)=T_s(t)\tilde{T}(k\mathscr{L}). \tag{11b}$$

Substituting into the spectral energy equation for isotropic turbulence

$$\frac{\partial E(k,t)}{\partial t}=T(k,t)-2\nu k^2E(k,t) \tag{12}$$

and enforcing consistency, he found

$$\mathscr{L}=\lambda, \tag{13a}$$

$$E(k,t)/q^2\lambda=\tilde{E}(k\lambda), \tag{13b}$$

$$T(k,t)/q^3=\mathrm{Re}_\lambda^{-1}\tilde{T}(k\lambda), \tag{13c}$$

and an arbitrary decay exponent n, where $\mathrm{Re}_\lambda=q\lambda/\nu$ is the Reynolds number based on turbulent velocity (q) and Taylor's microscale. Corresponding results were obtained earlier by Barenblatt and Gavrilov[19] using an equivalent similarity hypothesis for the double and the triple correlation coefficients. With the Re_λ^{-1} modification, any decay exponent is now consistent. However, this modification implies stronger nonlinear interactions with decreasing Reynolds number, which is not physically reasonable. However, George[18] suspects that such a similarity might exist at an early stage of the decay during which the turbulence is still in developing and the nonlinear terms are increasing. The derivative skewness thus increases with decreasing Reynolds number and eventually reaches a maximum value. After that, possibly another self-similar state that includes the proper decay of nonlinear terms is entered.

In the present study, we develop a new self-similarity that satisfies the Kármán–Howarth equation, is consistent with a power-law energy decay with an arbitrary decay exponent, and is physically reasonable. We believe that this new self-similarity is applicable to fully developed turbulence.

B. Proposed similarity

We recall that the evolution equations for energy and dissipation rate are

$$\dot{K} \equiv -\epsilon = -10\nu K/\lambda^2, \tag{14a}$$

$$\dot{\epsilon} = \frac{\epsilon^2}{K}\left(\frac{7}{30} S\ \mathrm{Re}_\lambda - \frac{7}{15} G\right), \tag{14b}$$

where $S \equiv -\lambda^3 k_0'''$ is the skewness of longitudinal velocity derivatives and $G \equiv \lambda^4 f_0^{\mathrm{IV}}$. If a power-law decay exists, i.e., there exists an n and a time reference t_o such that

$$K \sim (t+t_o)^{-n} \text{ and so } \epsilon \sim (t+t_o)^{-n-1}. \tag{15}$$

Equation (14b) then implies that the quantity in the bracket has to be a constant. In other words, we must have

$$G = \frac{1}{2} S\ \mathrm{Re}_\lambda + \frac{15}{7}\frac{(n+1)}{n}. \tag{16}$$

Therefore, similarity solutions of the form given by (8) (constant Re_λ, S, and $n=1$) or of the form given by (13) ($S \sim \mathrm{Re}^{-1}$) both imply a constant G during the decay. We consider the possibility of a nonconstant G and insist on a power-law dependence on Re_λ of the skewness S. Based on (16), we propose a complete similarity of the following form:

$$f(r,t) = f_1(r/\lambda) + \mathrm{Re}_\lambda^\beta f_2(r/\lambda) \tag{17a}$$

and

$$k(r,t) = \mathrm{Re}_\lambda^{\beta-1} k_2(r/\lambda). \tag{17b}$$

Since $f(r,t)$ and $k(r,t)$ are related to $E(k,t)$ and $T(k,t)$ by

$$E(k,t) = \frac{q^2}{\pi}\int_0^\infty kr(\sin kr - kr\cos kr) f(r,t)\,dr \tag{18a}$$

and

$$T(k,t) = \frac{q^3}{\pi}\int_0^\infty k^2 r\left(\frac{3\sin kr}{kr} - 3\cos kr - kr\sin kr\right) \times k(r,t)\,dr, \tag{18b}$$

the above hypothesis is equivalent to assuming self-similarity of the energy and energy transfer spectra of the form

$$E(k,t)/q^2\lambda = E_1(k\lambda) + \mathrm{Re}_\lambda^\beta E_2(k\lambda), \tag{19a}$$

$$T(k,t)/q^3 = \mathrm{Re}_\lambda^{\beta-1} T_2(k\lambda), \tag{19b}$$

where E_1, E_2, and T_2 are the self-similar functions related to f_1, f_2, and k_2, respectively.

Substituting (17a) and (17b) into (16) and (7), and using relations (14a), we obtain

$$G = \left.\frac{d^4 f_1}{d\zeta^4}\right|_{\zeta=0} + \left.\frac{d^4 f_2}{d\zeta^4}\right|_{\zeta=0} \cdot \mathrm{Re}_\lambda^\beta = \frac{15}{7}\frac{(n+1)}{n} - \left.\frac{1}{2}\frac{d^3 k_2}{d\zeta^3}\right|_{\zeta=0} \cdot \mathrm{Re}_\lambda^\beta \tag{20}$$

and

$$\left[10 f_1 + \frac{5}{n}\zeta\frac{df_1}{d\zeta} + \frac{2}{\zeta^4}\frac{d}{d\zeta}\left(\zeta^4\frac{df_1}{d\zeta}\right)\right] + \mathrm{Re}_\lambda^\beta \cdot \frac{1}{\zeta^4}\frac{d}{d\zeta}(\zeta^4 k_2) + \mathrm{Re}_\lambda^\beta \cdot \left[\left(10 + 5\beta - \frac{5}{n}\beta\right) f_2 + \frac{5}{n}\zeta\frac{df_2}{d\zeta} + \frac{2}{\zeta^4}\frac{d}{d\zeta}\left(\zeta^4\frac{df_2}{d\zeta}\right)\right] = 0, \tag{21}$$

where $\zeta \equiv r/\lambda$. From (20), we require

$$\left.\frac{d^4 f_1}{d\zeta^4}\right|_{\zeta=0} = \frac{15}{7}\cdot\frac{(n+1)}{n} \tag{22a}$$

and

$$\left.\frac{d^4 f_2}{d\zeta^4}\right|_{\zeta=0} = -\frac{1}{2}\left.\frac{d^3 k_2}{d\zeta^3}\right|_{\zeta=0}. \tag{22b}$$

If $\beta=0$, we recover George's self-similarity.[18] On the other hand, if $\beta \neq 0$, f_1, f_2, and k_2 must satisfy

$$10 f_1 + \frac{5}{n}\zeta\frac{df_1}{d\zeta} + \frac{2}{\zeta^4}\frac{d}{d\zeta}\left(\zeta^4\frac{df_1}{d\zeta}\right) = 0 \tag{23a}$$

and

$$\left(10 + 5\beta - \frac{5}{n}\beta\right) f_2 + \frac{5}{n}\zeta\frac{df_2}{d\zeta} + \frac{2}{\zeta^4}\frac{d}{d\zeta}\left(\zeta^4\frac{df_2}{d\zeta}\right) + \frac{1}{\zeta^4}\frac{d}{d\zeta}(\zeta^4 k_2) = 0. \tag{23b}$$

Equation (23a) is the same equation as that governing a complete self-similar $f(r/\lambda)$ when the triple correlation coefficient $k(r,t)$ in the Kármán–Howarth relation is ignored.[20] It is known that (23a) has solutions for all $n \in (0,\infty)$ and function f_1 can be expressed in terms of the regular confluent hypergeometric function

$$f_1(\zeta) = M\left(n, \frac{5}{2}, -\frac{5}{4n}\zeta^2\right) \tag{24}$$

under the conditions

$$f_1(0) = 1, \quad f_1(\infty) = 0. \tag{25}$$

Moreover,

$$\frac{5}{n} = 5 - 3 \Big/ \int_0^\infty \zeta f_1(\zeta)\,d\zeta, \tag{26}$$

provided $f_1 \to 0$ as $\zeta \to \infty$ at least faster than ζ^{-2}.

Although (23b) is not closed, we can write f_2 in terms of an integral involving the unknown function k_2 as follows:

$$f_2(\zeta)=-M(a,b,z)\int_0^z \frac{U(a,b,z')h(z')}{M(a,b,z')U'(a,b,z')-M'(a,b,z')U(a,b,z')}\,dz'$$

$$+U(a,b,z)\int_0^z \frac{M(a,b,z')h(z')}{M(a,b,z')U'(a,b,z')-M'(a,b,z')U(a,b,z')}\,dz', \tag{27a}$$

with

$$z\equiv-\frac{5}{4n}\zeta^2,\quad a\equiv n+\frac{\beta(n-1)}{2},\quad b\equiv\frac{5}{2}, \tag{27b}$$

and

$$h(z)\equiv-\frac{2n^2}{25}\cdot\left[\frac{5k_2(\zeta)}{\zeta^3}+\frac{1}{\zeta}\frac{d}{d\zeta}\left(\frac{k_2(\zeta)}{\zeta}\right)\right] \tag{27c}$$

under the conditions

$$f_2(0)=0,\quad f_2(\infty)=0, \tag{28}$$

where $U(a,b,z)$ is the singular confluent hypergeometric function and $k_2(\zeta)$ is assumed to be an odd function of ζ. Expanding (23b) about $\zeta=0$ with (28), we find that

$$f_2(\zeta)\sim-\frac{1}{48}\left.\frac{d^3k_2}{d\zeta^3}\right|_{\zeta=0}\cdot\zeta^4+\mathcal{O}(|\zeta|^6). \tag{29}$$

Condition (22b) is therefore satisfied implicitly. Condition (22a) follows by differentiating (23a) twice and evaluating the results at $\zeta=0$. We now have a consistent theory with two free parameters n and β, and one function that must be determined.

In some cases, it is possible to fix n by using the asymptotic behaviors of $f_1(\zeta)$ and $f_2(\zeta)$, as $\zeta\to\infty$ predicted by earlier investigators.[12,14] In particular, consider Saffman's result[12] that $f(r,t)$, in general, has a power-law asymptotic behavior, given by

$$f(r,t)\sim r^{-3}\quad\text{as}\quad r\to\infty. \tag{30}$$

The asymptotic behaviors of functions $f_1(\zeta)$ and $f_2(\zeta)$ can be obtained from (24) and (27a). As $\zeta\to\infty$, it can be shown that

$$f_1(\zeta)\sim\zeta^{-2n} \tag{31a}$$

and

$$f_2(\zeta)\sim\zeta^{-[2n+\beta(n-1)]}, \tag{31b}$$

provided those integrals involved with $k_2(\zeta)$ in the solutions of f_2 converge rapidly enough. Solutions of f_1 corresponding to several values of n within interest are shown in Fig. 1. They are found everywhere positive implying from (26) $n\geqslant 1$. With $n\geqslant 1$ and $\beta\geqslant 0$, we obtain

$$f(r,t)\sim f_1(\zeta)\sim\zeta^{-2n}\quad\text{as}\quad\zeta\to\infty, \tag{32}$$

giving $n=1.5$ if we envoke (30).

In summary, a complete similarity hypothesis of the velocity correlation coefficients given by

$$f(r,t)=M\left[n,\frac{5}{2},-\frac{5}{4n}\left(\frac{r}{\lambda}\right)^2\right]+\mathrm{Re}_\lambda^{\beta}\,f_2\left(\frac{r}{\lambda}\right) \tag{33a}$$

and

$$k(r,t)=\mathrm{Re}_\lambda^{\beta-1}\,k_2\left(\frac{r}{\lambda}\right) \tag{33b}$$

is proposed with f_2 and k_2 related by (27).

III. NUMERICAL SIMULATIONS

In this section, we study the decay of turbulence by numerical simulation and compare the results with the theories discussed in the previous section.

A. Numerical methods and initial conditions

We use the Fourier spectral method. The velocity components are expanded in terms of their Fourier coefficients,

$$\mathbf{u}(\mathbf{x},t)=\sum_{\mathbf{k}}\hat{\mathbf{u}}(\mathbf{k},t)\exp(i\mathbf{k}\cdot\mathbf{x}). \tag{34}$$

The Fourier coefficients of the nonlinear terms in the Navier–Stokes equations are obtained by forming the products of velocity components and velocity gradients in the physical space and transforming back to the wave space. The Fourier coefficients of the pressure are combined with those of the nonlinear terms by taking advantage of the incompressibility condition. The resulting spectral Navier–Stokes equations are

$$\frac{\partial\hat{u}_i}{\partial t}+(\delta_{ij}-k_ik_j/k^2)\cdot ik_m\widehat{(u_mu_j)}+\nu k^2\hat{u}_i=0, \tag{35}$$

where δ_{ij} is the Kronecker delta.

Time advancing is by second-order Runge–Kutta. Aliasing errors are approximately eliminated through the use of the grid shift technique[21] and a special treatment of the time

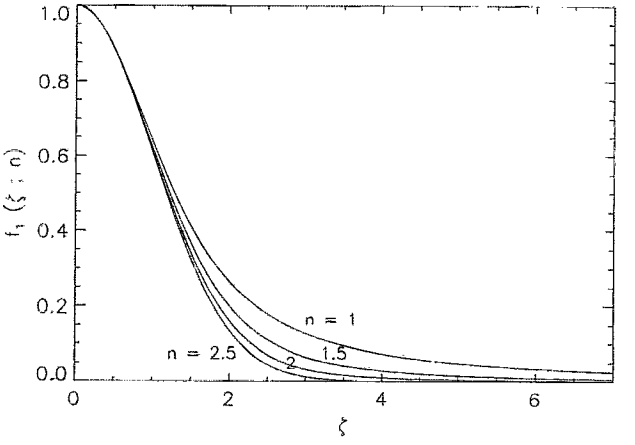

FIG. 1. Confluent hypergeometric function $f_1(\zeta)=M[n,5/2,-(5/4n)\zeta^2]$ with $n=1$, 1.5, 2, and 2.5.

TABLE I. Initial conditions and conditions at start of power-law decay.

	run1	run2	run3	run4	run5	run6	run7
symbol	●	○	+	■	◇	△	*
time=0							
k_pL	20π	40π	32π	16π	16π	24π	24π
$E(k,0)$	Eq. (36a)	Eq. (36a)	Eq. (36a)	Eq. (36b)	Eq. (36b)	Eq. (36c)	Eq. (36c)
ν	0.0015	0.0015	0.0003	0.002	0.0004	0.0013	0.003
N	128	256	256	256	256	256	256
Re_λ	133	133	667	203	348	165	72
$k_{\max}\eta$	0.53	0.53	0.47	0.40	0.39	0.51	0.78
$\mathscr{T}_0$	0.59	0.59	0.25	0.21	0.22	0.40	0.39
time power-law decay begins							
$k_{\max}\eta$	1.09	1.09	1.00	1.00	0.99	1.03	1.09
Re_λ	21.5	21.6	44.6	46.2	49.6	42.6	28.0
λ/L	2.6%	1.3%	1.7%	1.8%	1.8%	1.8%	1.5%
$\mathscr{T}_0$	1.91	1.84	3.14	1.80	2.80	2.89	1.16
τ_η	0.22	0.22	0.23	0.14	0.17	0.22	0.11
time $\lambda/L\approx 10\%$							
$k_{\max}\eta$	5.92	14.08	8.11	8.22	>3.96	>6.00	9.18
Re_λ	10.8	7.6	19.8	22.1	<35.3	<27.1	17.6
n	1.56	1.51	1.42	1.31	1.23	1.27	1.24
t_0	0.40	0.064	−0.88	−0.14	−1.28	0.45	0.16

differencing.[22] The algorithm used was originally developed by Rogallo[22] and subsequently parallelized to run on the Intel Delta parallel computer at Caltech.

All of the simulations start from a random velocity field in a periodic domain of size L on a side, with a specified initial energy spectrum. Initial energy spectra were chosen from

$$E(k,t=0)=16\sqrt{\frac{2}{\pi}}\frac{q^2}{k_p}\left(\frac{k}{k_p}\right)^4\exp\left[-2\left(\frac{k}{k_p}\right)^2\right], \tag{36a}$$

or

$$E(k,t=0)=\begin{cases} Cq^2\exp(-a)(k/k_p)^2 & \text{for } 0\leqslant k\leqslant k_p; \\ Cq^2(k/k_p)^{-5/3}\exp(-ak/k_p) & \text{for } k\geqslant k_p, \end{cases} \tag{36b}$$

or

$$E(k,t=0)=\frac{3}{2}\frac{q^2}{k_p}\left(\frac{2k}{k_p}\right)^2\exp\left(-\frac{2k}{k_p}\right), \tag{36c}$$

where all spectra have a peak at $k=k_p$. Parameters used in each simulation and certain dynamical quantities at the initial time and at the time the power-law decay appears to begin are listed in Table I. Included are the product of the maximum available wave number $k_{\max}=(\sqrt{2}N/3)\cdot(2\pi/L)$ (N is the resolution, i.e., the number of grid points in each direction) and Kolmogorov's dissipation length scale η, Re_λ, the eddy turnover time, and the eddy dissipation time. The eddy-turnover time, $\mathscr{T}_0$, and the dissipation time scale, τ_η, are defined as

$$\mathscr{T}_0\equiv\frac{3\pi}{4q}\frac{\int_0^\infty k^{-1}E(k,t)dk}{\int_0^\infty E(k,t)dk} \tag{37}$$

and

$$\tau_\eta\equiv\eta^2/\nu, \tag{38}$$

respectively.

Note that to produce reasonably high Re_λ when the turbulence reaches the state of power-law decay, the initial values of $k_{\max}$ are chosen relatively small giving rather poor resolution during the initial stage of development. However, we do not use the data from this stage.

B. Power-law energy decay

The evolutions of turbulent energy K and those of Re_λ are shown in Figs. 2 and 3. The existence of a power-law decay is clear. The solid lines are the fitted curves of the form

$$K=K_o(t+t_o)^{-n} \tag{39}$$

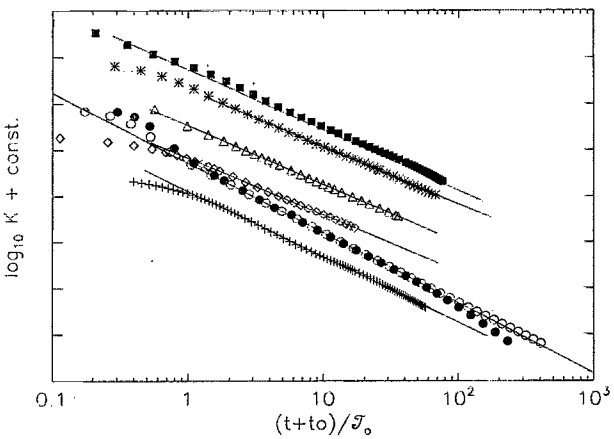

FIG. 2. The decay of turbulent energy K. $\mathscr{T}_0$ is the eddy turnover time at $k_{\max}\eta\approx 1$.

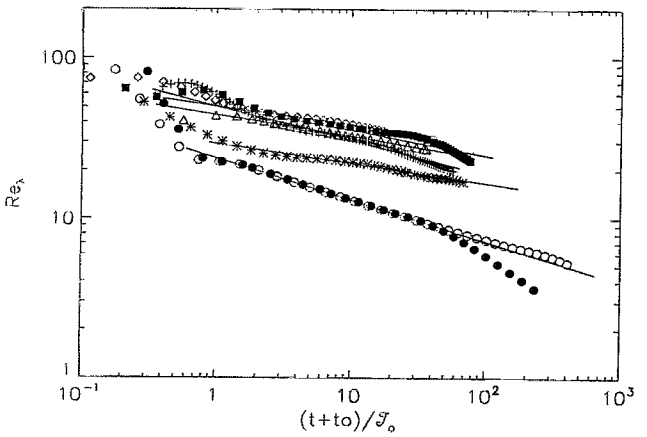

FIG. 3. The decay of Re_λ. $\mathcal{T}_o$ is the eddy turnover time at $k_{max}\eta \approx 1$. Solid lines are $Re_\lambda = \sqrt{20K_o/3\nu n}(t+t_o)^{(1-n)/2}$.

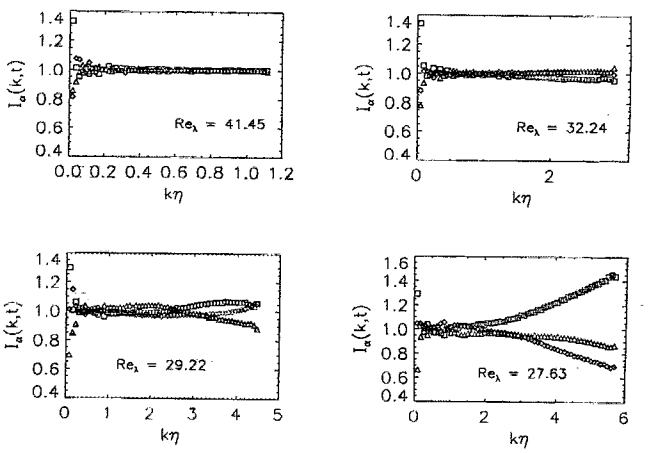

FIG. 5. The extent of isotropy of turbulence indicated by $I_\alpha(k,t)$ (run6).

with choices of K_o, t_o, and n which give the least square errors to those data between times during which $k_{max}\eta \geq 1$ and $\lambda/L \leq 0.1$. Values of t_o and n used can be found in Table I. In Fig. 3 the solid lines represent Re_λ in terms of the power-law parameters determined from Fig. 2, so that

$$Re_\lambda(t) = \sqrt{20K_o/3\nu n}(t+t_o)^{(1-n)/2}. \tag{40}$$

Moreover, for power-law decay we expect $\lambda^2 = 10\nu(t+t_o)/n$. The asymptotic time independence of $\lambda/\sqrt{t+t_o}$ is shown in Fig. 4.

We notice that in these figures the numerical data in some cases deviates from the fitted curves at large times. We believe that, in some cases, this occurs because the large eddies eventually become too large relative to the box size. A case in point is run1 (Fig. 2) which shows this effect, whereas run2 with twice the box dimension but the same initial spectrum as run1 does not show this effect.

Before we can compare the numerical results with isotropic turbulence theories, we need to check the extent of isotropy of the turbulence. Consider the one-dimensional energy spectrum defined as

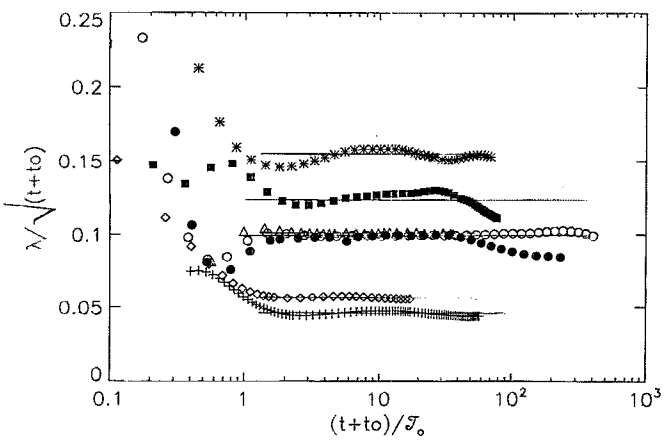

FIG. 4. The evolution of $\lambda/(t+t_o)^{1/2}$. $\mathcal{T}_o$ is the eddy turnover time at $k_{max}\eta \approx 1$ and solid lines are $\sqrt{10\nu/n}$ with n given in Table I.

$$E_\alpha(k,t) \equiv \frac{1}{2}\sum_{|\mathbf{k}|=k} \hat{u}_\alpha \hat{u}_\alpha^*(\mathbf{k},t), \tag{41}$$

where $\alpha = 1,2,3$. The extent of isotropy is measured by $I_\alpha(k,t)$ defined as

$$I_\alpha(k,t) \equiv 3E_\alpha(k,t)/E(k,t). \tag{42}$$

For isotropic turbulent flow, we expect $I_\alpha(k,t)$ to be close to one. The distributions of $I_\alpha(k,t)$ over the wave number k at several Re_λ for run6 are shown in Fig. 5. The large-scale eddies are never isotropic while the small-scale eddies lose isotropy as Reynolds number decreases, which must be caused by the formation of small-scale structures and their small sample in a single realization. This anisotropy should be kept in mind for the discussions below.

In the present study, the quantities G and S are computed as

$$G = \frac{2}{35}\frac{\lambda^4}{q^2}\int_0^\infty k^4 E(k,t)dk \tag{43}$$

and

$$S = -\frac{6\sqrt{15}}{7}\frac{\int_0^\infty k^2 T(k,t)dk}{(2\int_0^\infty k^2 E(k,t)dk)^{3/2}}. \tag{44}$$

From the relation (16) with computed Re_λ, G, and S, we can also compute the decay exponent as follows:

$$n^{-1} = \tfrac{7}{15}(G - \tfrac{1}{2}S\ Re_\lambda) - 1. \tag{45}$$

These three quantities are all plotted as a function of Re_λ in the range investigated (see Figs. 6–8). Similar plots of S have been done by Kerr,[7] as well as Mansour and Wray.[6] Again only those data between times during which $k_{max}\eta \geq 1$ and $\lambda/L \leq 0.1$ are plotted. In this way, we obtain a reasonable representation of the dissipation range and minimize the contamination due to periodicity. Except for some transitional early-time behavior (which may correspond to George's similarity regime), a nearly linear dependence on Re_λ of G and a nearly constant S are observed for each run during the

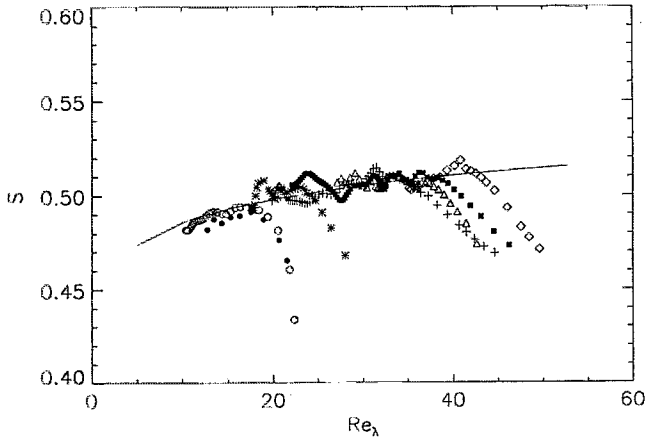

FIG. 6. S plotted as a function of Re_λ during $k_{\max}\eta \geqslant 1$ and $\lambda/L \leqslant 0.1$. The solid line is the fitted curve of the form $S = C\,\mathrm{Re}_\lambda^{\beta-1}$ with $C=0.44$ and $\beta=1.04$.

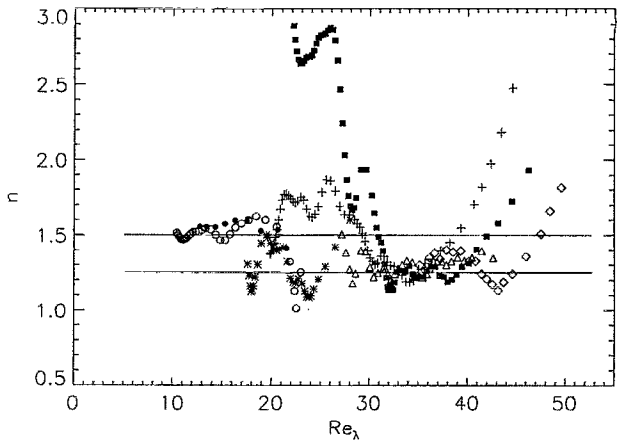

FIG. 8. The decay exponent n calculated by using Eq. (45) plotted as a function of Re_λ during $k_{\max}\eta \geqslant 1$ and $\lambda/L \leqslant 0.1$. Horizontal lines represent decay exponents of 1.5 and 1.25.

decay, implying $\beta \approx 1$. Note, also included in Fig. 7 is the data taken from Fig. 16 of Yeung and Pope[23] for stationary forced turbulence.

It is, in general, believed that the decay exponent is dominated by the large-scale motion or the spectral behavior of the energy spectrum at low wave numbers, especially during the initial period of decay. For example, Mansour and Wray[6] attempted to classify flows and their decay exponents according to the initial spectral behaviors at low wave numbers such as $E(k,0) \sim C_0 k^2$ and $E(k,0) \sim C_2 k^4$, where C_0 and C_2 are constants. From the present numerical data (Fig. 8), we observe two states with distinct decay exponents, one for Re_λ in the range of (30, 40) (run3, run5, and run6) and the other for Re_λ in (10, 20) (run2), and a transition between these two states as suggested by data of run3 (+), run4 (■), and run7 (*). This indicates a dependence of the decay exponent on Re_λ rather than on the spectral behavior at low wave numbers. Notice that run2 and run3 have an $E(k,0) \sim C_2 k^4$ while run5 and run6 have an $E(k,0) \sim C_0 k^2$. However, for the present simulations, the statistical sample at low wave numbers is especially small after the power-law decay begins so that a definitive statement on the influence of the spectral behavior cannot be made at this time.

Finally, the decay exponents, 1.5 and 1.25, are shown in Fig. 8 as horizontal lines. Recall that run2 yielded an exponent of 1.51 and the latter exponent, 1.25, is the average of run5 and run6 from Table I. The decay exponents from Table I are generally in good agreement with those computed from (45), giving assurance that we are observing isotropic, power-law decay.

C. Self-similarity

Finally, we attempt to test the similarity of the form proposed, that is, to test the existence of the self-similar functions $f_2(r,\lambda)$ and $k_2(r/\lambda)$. The correlations $f(r,t)$ and $k(r,t)$ in the present study are obtained by computing the velocity structure function

$$\Delta u_\alpha(r) \equiv u_\alpha(\mathbf{x}+r\mathbf{e}_\alpha) - u_\alpha(\mathbf{x}), \tag{46}$$

where $\mathbf{e}_\alpha$, $\alpha=1,2,3$, are the unit vectors in the Cartesian coordinates, and using the isotropic relations (in spite of the anisotropy observed above)

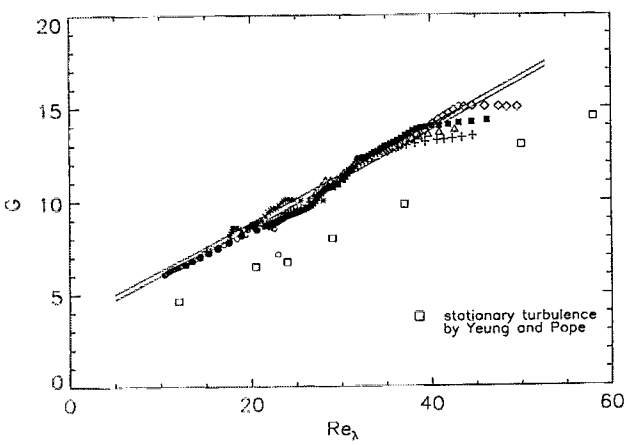

FIG. 7. G plotted as a function of Re_λ during $k_{\max}\eta \geqslant 1$ and $\lambda/L \leqslant 0.1$. The lower solid line is Eq. (16) with $n=1.5$ while the upper one with $n=1.25$.

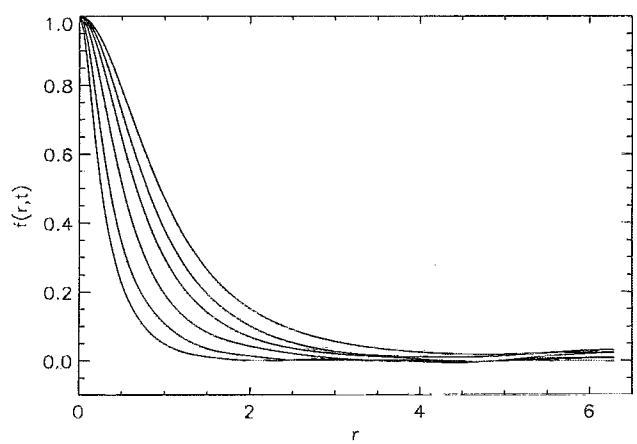

FIG. 9. Double velocity correlation coefficient, $f(r,t)$ for run2.

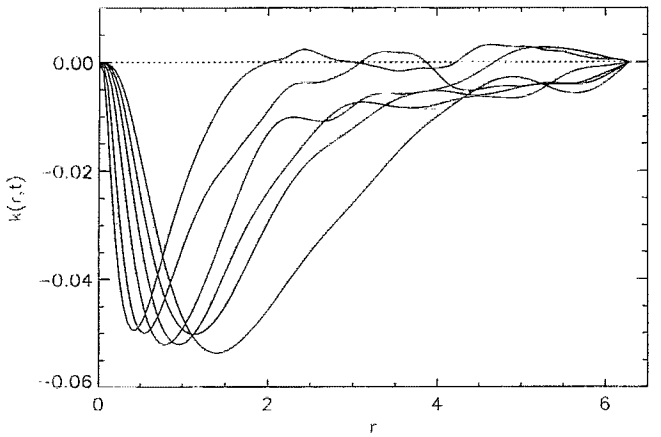

FIG. 10. Triple velocity correlation coefficient $k(r,t)$ for run2.

$$f(r,t)=1-\overline{\Delta u(r)^2}/2q^2 \tag{47}$$

and

$$k(r,t)=\overline{\Delta u(r)^3}/6q^3. \tag{48}$$

Averaging is taken over the full volume and over the three directions. Examples are shown in Fig. 9 for $f(r,t)$ and in Fig. 10 for $k(r,t)$. Note the double correlation $f(r,t)$ can also be obtained by measuring the one-dimensional energy spectra and taking the Fourier transform. We found the results agree with those of (47). The zeros of $k(r,t)$ at $r=0$, $\pm L/2$ come directly from (48) and the periodicity of the flow field. The relatively high values of function $f(r,t)$ shown in Fig. 9 for $r\approx L/2$ at later times indicate the box-size contamination once again. The persistence of the peak values of function $k(r,t)$ implies the presence of the inertial forces for all time, and so the so-called final period of decay is not observed in the range of Re_λ investigated in agreement with Mansour and Wray.[6]

We select run2, run5, and run6 for testing, corresponding to the two distinct decay exponents that are observed. The decay exponent $n=1.5$ is used for run2 while $n=1.25$ for run5 and run6. Note, run5 and run6 are expected to possess the same self-similar functions f_2 and k_2. To determine the value of β, we use all the data for S in Fig. 6, except those in the early transient period. Note the data for S in Fig. 6 could be described by $S\approx\text{const}\approx 0.50$ or by

$$S\sim \mathrm{Re}_\lambda^{\beta-1} \tag{49}$$

with $\beta=1.04$ as shown by the solid curve. With the latter fit and the use of the two decay exponents 1.5 and 1.25, we plot two curves for G given by (16) in Fig. 7. Again we see consistency with the results for G computed directly by (43). Use of $S=\text{const}=0.50$ rather makes only a slight change in the curves shown in Fig. 7.

In Fig. 11 we show double velocity correlation coefficients f as a function of r/λ for the three runs. Figures 12(a) and 13(a) show the result of subtracting $f_1(r/\lambda)$ from $f(r/\lambda,t)$. Next we divide the above results by $\mathrm{Re}_\lambda^\beta$ with $\beta=1.04$ to obtain our estimate for $f_2(r/\lambda)$. This is shown in Figs. 12(b) and 13(b). Although some spread in the curves persists, it is clearly reduced from the spread shown in Figs. 12(a) and 13(a). The difference between the f_2 functions of the two cases is clearly much larger than its spread in each.

Similarly we show $k(r,t)$ in its proposed self-similar form in Fig. 14. Here the collapse of the data is reasonably good but not as good as it was with the double correlation coefficients where two functions $f_1(r/\lambda)$ and $f_2(r/\lambda)$ are used.

D. Discussion

We have studied three completely self-similar solutions of Kármán–Howarth equation: Kármán–Howarth's $[f(r,t)=\tilde{f}(r/\lambda), k(r,t)=\tilde{k}(r/\lambda)$, and $n=1]$, George's $[f(r,t)=\tilde{f}(r/\lambda)$ and $k(r,t)=\mathrm{Re}_\lambda^{-1}\tilde{k}(r/\lambda)]$, and the one proposed herein $[f(r,t)=f_1(r/\lambda)+\mathrm{Re}_\lambda^\beta f_2(r/\lambda)$ and $k(r,t)=\mathrm{Re}_\lambda^{\beta-1}k_2(r/\lambda)]$. The solution proposed herein is the only one that can predict a decreasing nonlinear interaction during the decay with $\beta>1$ and thus is the only one that might be applied to the

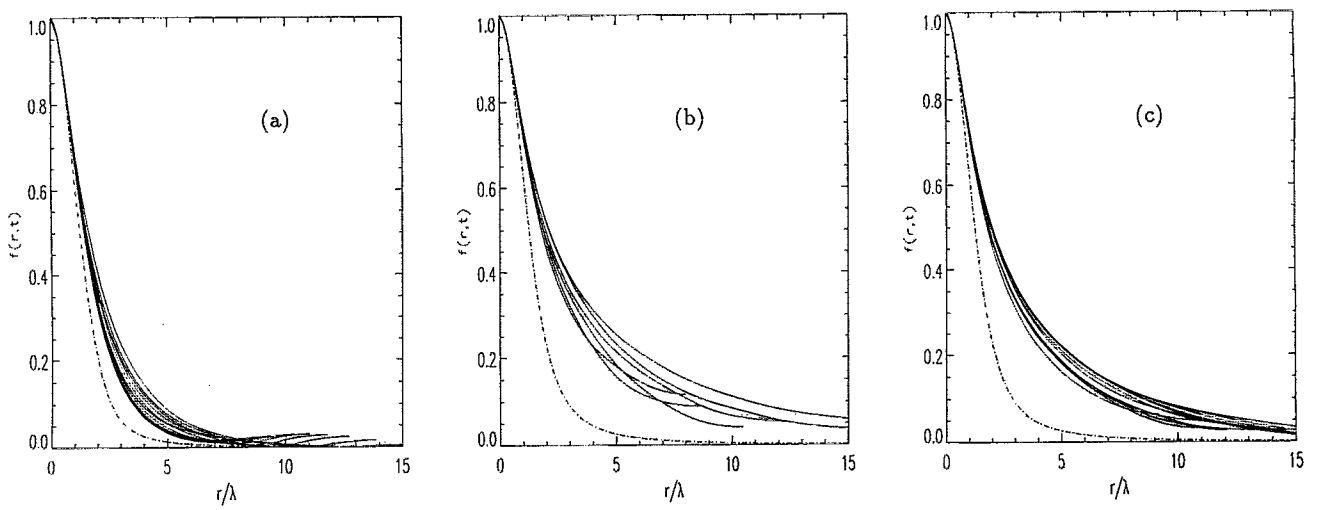

FIG. 11. Double velocity correlation coefficients $f(r/\lambda,t)$ (solid lines) for (a) run2 ($n=1.5$), (b) run5 ($n=1.25$), (c) run6 ($n=1.25$). The dash–dotted lines are the regular confluent hypergeometric function $M(n,5/2,-5\zeta^2/4n)$, where $\zeta=r/\lambda$.

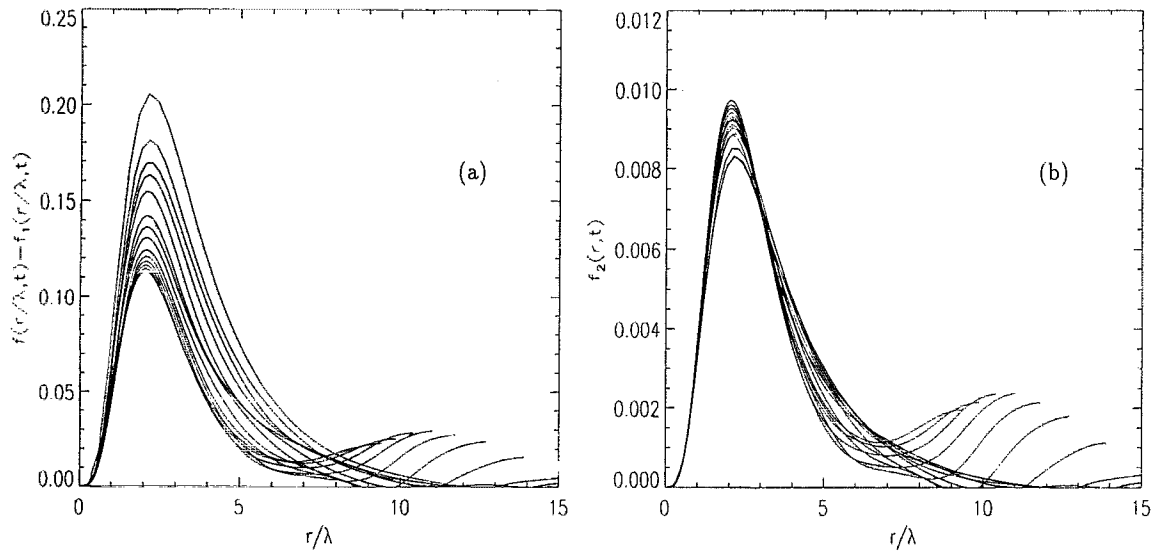

FIG. 12. (a) $f(r/\lambda,t)-f_1(r/\lambda)$, (b) $f_2(r/\lambda)$, for run2 with $\beta=1.04$ and $n=1.5$.

final period of decay. The self-similar functions f_1, f_2, and k_2, however, depend on the decay exponent n, which in turn depends on the initial conditions and possibly the Reynolds number as well. George's similarity which can be treated as a special case with $\beta=0$ is possibly a self-similar state for an early stage of decay during which turbulence is still developing and the skewness has not yet reached its maximum value. A modification of George's similarity which gives explicitly a maximum skewness S during the decay and is consistent with the relation (16) is actually obtainable and is presented in the Appendix. Such a similarity, however, like George's, cannot be applied to the final period of decay.

It has been argued that Kármán–Howarth's solution is a limiting solution at infinite Reynold number (Barenblatt and Gavrilov[19] and George[18]) and also a limiting solution as Reynolds number goes to zero (Speziale and Bernard[9]). The latter case is not meaningful because it requires $K\rightarrow 0$. The former case is argued on the empirical grounds and the fact that the Kolmogorov similarity law can be satisfied in this solution ($n=1$). In particular, all length scales are proportional for all time in this special solution because the Reynolds number remains constant during the decay. However, we doubt the applicability of the $n=1$ solution and, in fact, our proposed similarity solution at large Reynolds number, because only one length scale is used. For such a flow, we suspect that two length scales must be employed, an energy scale $\mathscr{L}\equiv q^3/\epsilon\propto\lambda\ \mathrm{Re}_\lambda$ and the Kolmogorov dissipation scale $\eta\equiv(\nu^3/\epsilon)^{1/4}\propto\lambda\ \mathrm{Re}_\lambda^{-1/2}$, well separated because $\mathrm{Re}_\lambda\gg 1$. (Even though the Reynolds number is constant in time for the $n=1$ solution, it can vary from one flow to another and we require universality of the similarity solution.) Thus we believe the

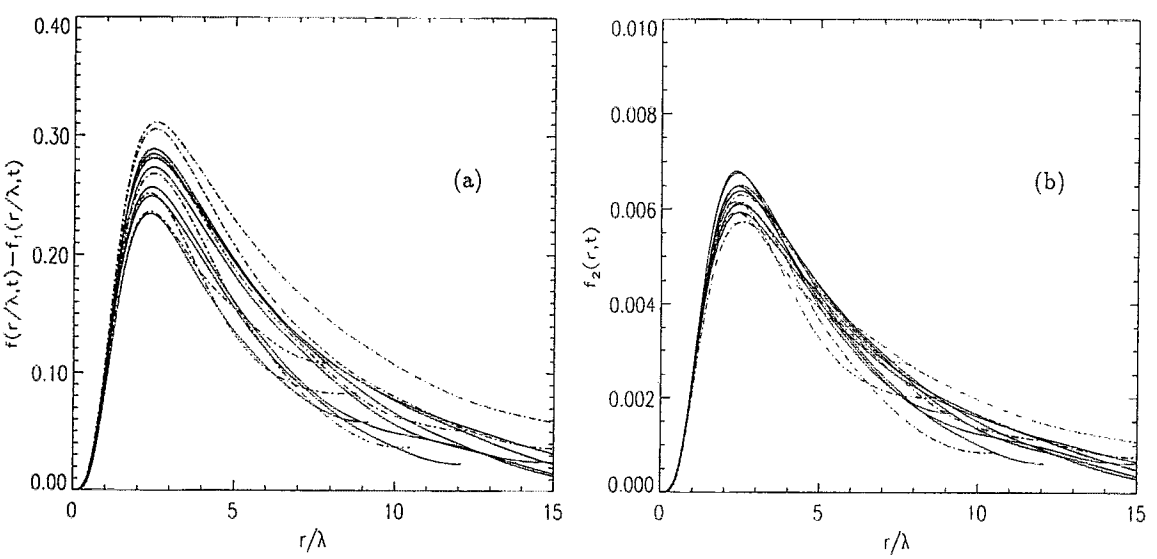

FIG. 13. (a) $f(r/\lambda,t)-f_1(r/\lambda)$, (b) $f_2(r/\lambda)$, for run5 (dash dotted lines) and run6 (solid lines) with $\beta=1.04$ and $n=1.25$.

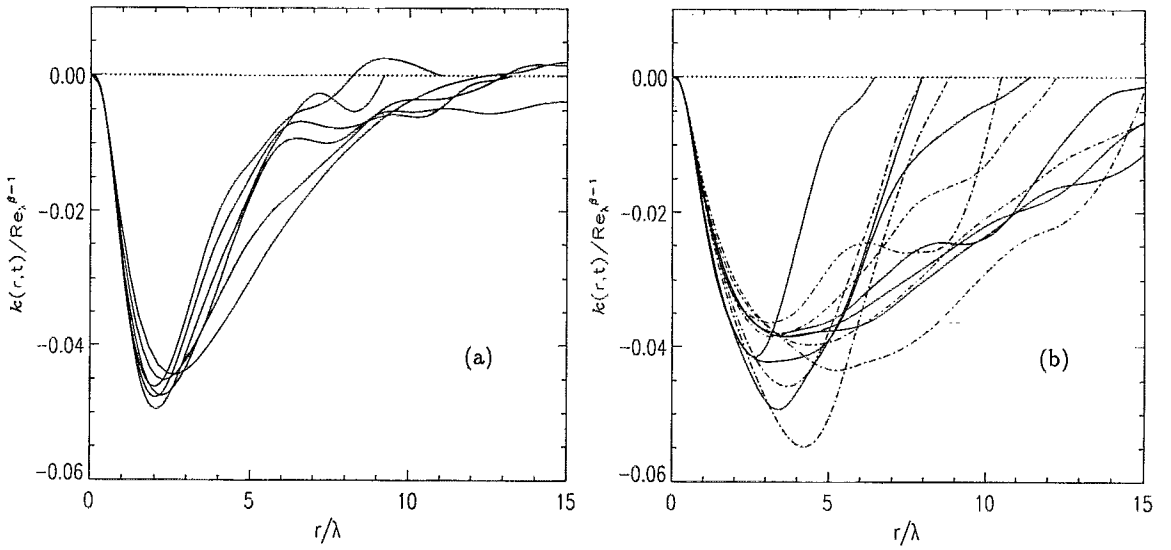

FIG. 14. Triple velocity correlation coefficients $k(r/\lambda,t)/\mathrm{Re}_\lambda^{\beta-1}$ with $\beta=1.04$ for (a) run2, (b) run5 (dash dotted lines), and run6 (solid lines).

leading terms for the two-point correlation function are given by

$$f(r)=f_{10}\left(\frac{r}{\lambda\ \mathrm{Re}_\lambda}\right)+\mathrm{Re}_\lambda^{-2}\cdot f_{11}\left(\frac{r}{\lambda\ \mathrm{Re}_\lambda}\right)+\mathrm{Re}_\lambda^{-1}\cdot f_{20}\left(\frac{r\ \mathrm{Re}_\lambda^{1/2}}{\lambda}\right)+\mathrm{Re}_\lambda^{-2}\cdot f_{21}\left(\frac{r\ \mathrm{Re}_\lambda^{1/2}}{\lambda}\right), \tag{50}$$

corresponding to an energy spectrum given by

$$E(k)=q^2\lambda\ \mathrm{Re}_\lambda\cdot[E_{10}(k\lambda\ \mathrm{Re}_\lambda)+\mathrm{Re}_\lambda^{-2}\cdot E_{11}(k\lambda\ \mathrm{Re}_\lambda)]+q^2\lambda\ \mathrm{Re}_\lambda^{-3/2}\cdot[E_{20}(k\lambda\ \mathrm{Re}_\lambda^{-1/2})+\mathrm{Re}_\lambda^{-1}\cdot E_{21}(k\lambda\ \mathrm{Re}_\lambda^{-1/2})]. \tag{51}$$

The triple correlation function would be given by

$$k(r)=k_{10}\left(\frac{r}{\lambda\ \mathrm{Re}_\lambda}\right)+\mathrm{Re}_\lambda^{-2}\cdot k_{11}\left(\frac{r}{\lambda\ \mathrm{Re}_\lambda}\right)+\mathrm{Re}_\lambda^{-3/2}\cdot k_{20}\left(\frac{r\ \mathrm{Re}_\lambda^{1/2}}{\lambda}\right)+\mathrm{Re}_\lambda^{-5/2}\cdot k_{21}\left(\frac{r\ \mathrm{Re}_\lambda^{1/2}}{\lambda}\right). \tag{52}$$

In the Kármán–Howarth equation, the function f_{10} would yield the leading-order term for the time derivative of $f(r)$ and be balanced by the k_{10} component of $k(r)$, and f_{20} would yield the leading order contribution for the dissipation term in the equation and be balanced by k_{20}.

It is interesting to compare the small r expansion of the proposed high Re_λ representation of $f(r)$ given by (50) with the expansion of our proposed similarity form (17a). The expansion of the latter is given by

$$f(r)=1-\frac{r^2}{2\lambda^2}+\{C_1+C_2\ \mathrm{Re}_\lambda^\beta\}\left(\frac{r}{\lambda}\right)^4+\{C_3+C_4\ \mathrm{Re}_\lambda^\beta\}\times\left(\frac{r}{\lambda}\right)^6+\cdots; \tag{53}$$

while the former is given by

$$f(r)=1-\frac{r^2}{2\lambda^2}+[D_1+D_2\ \mathrm{Re}_\lambda+o(1)]\left(\frac{r}{\lambda}\right)^4+\{D_3\ \mathrm{Re}_\lambda+D_4\ \mathrm{Re}_\lambda^2+o(\mathrm{Re}_\lambda)\}\left(\frac{r}{\lambda}\right)^6+\cdots, \tag{54}$$

where C_i and D_i, $i=1, 2, 3, 4$, are all constants and conditions such as $f(0)=1$ and $-1/f''(0)=\lambda^2$ have been imposed. The similarity form (17a) seemingly still provides a good model with $\beta=1$ as a partially self-similar solution given by (50) for large Reynolds number, at least up to the order of $(r/\lambda)^6$. Finally, the representation of $k(r,t)$ given by (52) suggests a skewness given by

$$S=S_1+S_2\ \mathrm{Re}_\lambda^{-1}+o(\mathrm{Re}_\lambda^{-1}), \tag{55}$$

where S_1 and S_2 are constants.

IV. SUMMARY AND CONCLUSION

Simulations of decaying homogeneous turbulence at small to intermediate Reynolds numbers have been performed. We find that the turbulent kinetic energy decays eventually as a power law in time. The decay exponent for the initial conditions summarized in Sec. III A is found to be about 1.5 for Re_λ in (10, 20) and 1.25 for Re_λ in (30,40). A new self-similar form for the double and triple velocity correlations of decaying turbulence has been proposed in which the Taylor microscale is the appropriate scaling. The double correlation coefficient is divided into two parts—one has a power-law dependence on the Reynolds numbers and the other does not. The nonlinear terms, as measured by the triple velocity correlations, vary as $\mathrm{Re}_\lambda^{\beta-1}$ during the decay. Provided $\beta\neq0$, two independent equations can be obtained with three unknown functions. Although the problem is still not closed, the asymptotic behavior of $f(r,t)$ at large separation r is found uniquely related to the decay exponent n. Together with Saffman's proposed asymptotic behavior of

$f(r,t)$, the theory predicts a decay exponent of 1.5 in agreement with some of the present numerical results.

A nearly linear relation between Re_λ and G, a quantity related to the dissipation of enstrophy, was observed, in agreement with the observation that the skewness $S \sim \mathrm{Re}_\lambda^{\beta-1}$ with $\beta=1.04$. Because $\beta>1$ (so the inertial force increases as Reynolds number increases), the result may be applicable to the limiting case of zero Reynolds number—to the final period of decay in which the inertial effect is negligible and the double correlation coefficients approach a complete self-similar state.

On the other hand, we believe there exists an upper limit for the validity of the proposed similarity. At large Re_λ we anticipate at least two length scales will be required, the dissipation scale, $\eta \sim \lambda\, \mathrm{Re}_\lambda^{-1/2}$, and the energy scale, $\mathscr{L} \sim \lambda\, \mathrm{Re}_\lambda$.

ACKNOWLEDGMENTS

We thank Dr. Robert Rogallo for his generosity for providing the basic program for the simulations. He and Dr. Alan Wray provided valuable comments. We are also grateful to Professors P. E. Dimotakis, W. K. George, D. I. Pullin, and P. G. Saffman for stimulating discussions. This research was performed in part using the Intel Touchstone Delta System operated by Caltech on behalf of the Concurrent Supercomputing Consortium. This work was supported by the U.S. Air Force Office of Scientific Research under Grant No. AFOSR-91-0241.

APPENDIX: MODIFIED SIMILARITY HYPOTHESIS

A modification to the George's similarity which is consistent with (16) is discussed here. Instead of (17b), we consider

$$f(r,t)=f_1(r/\lambda)+\mathrm{Re}_\lambda^{\beta}\, f_2(r/\lambda) \tag{A1}$$

and

$$k(r,t)=\mathrm{Re}_\lambda^{-1}\, k_1(r/\lambda)+\mathrm{Re}_\lambda^{\beta-1}\, k_2(r/\lambda). \tag{A2}$$

The expression for G (16) and skewness S thus become

$$G=\left.\frac{d^4 f_1}{d\zeta^4}\right|_{\zeta=0}+\left.\frac{d^4 f_2}{d\zeta^4}\right|_{\zeta=0}\cdot \mathrm{Re}_\lambda^{\beta}=\left[\frac{15}{7}\left(\frac{n+1}{n}\right)-\frac{1}{2}\left.\frac{d^3 k_1}{d\zeta^3}\right|_{\zeta=0}\right]-\left.\frac{1 d^3 k_2}{2\, d\zeta^3}\right|_{\zeta=0}\cdot \mathrm{Re}_\lambda^{\beta} \tag{A3}$$

and

$$S=-\left.\frac{d^3 k_2}{d\zeta^3}\right|_{\zeta=0}\cdot \mathrm{Re}_\lambda^{\beta-1}-\left.\frac{d^3 k_1}{d\zeta^3}\right|_{\zeta=0}\cdot \mathrm{Re}_\lambda^{-1}. \tag{A4}$$

Two equations with four unknown functions are obtained if one substitutes (A1) and (A2) into Kármán–Howarth equation. The boundary condition (22a) of f_1 has been changed to

$$\left.\frac{d^4 f_1}{d\zeta^4}\right|_{\zeta=0}=\frac{15}{7}\left(\frac{n+1}{n}\right)-\left.\frac{1 d^3 k_1}{2\, d\zeta^3}\right|_{\zeta=0}. \tag{A5}$$

Most of all, provided $0<\beta<1$ and $d \equiv -k_1'''(0) < 0$ and $c \equiv -k_2'''(0) > 0$, a maximum S exists and occurs at $\mathrm{Re}_{\lambda *}=[d/c(\beta-1)]^{-1/\beta}$. With $S_{\max} = \beta d/(\beta-1)\cdot \mathrm{Re}_{\lambda *}^{-1}$, we obtain

$$\frac{S}{S_{\max}}=\frac{1}{\beta}\left[\left(\frac{\mathrm{Re}_\lambda}{\mathrm{Re}_{\lambda *}}\right)^{\beta-1}+(\beta-1)\left(\frac{\mathrm{Re}_\lambda}{\mathrm{Re}_{\lambda *}}\right)^{-1}\right]. \tag{A6}$$

If β is universal, Eq. (A6) then provides an universal relationship between $S/S_{\max}$ and $\mathrm{Re}_\lambda/\mathrm{Re}_{\lambda *}$. Although we have observed a transient state before turbulence becomes fully developed in Fig. 6 from all the simulations, we have difficulties in getting a maximum S and its corresponding $\mathrm{Re}_{\lambda *}$ because of the fluctuation of the data. Further simulations concentrating on this transient state are expected to be performed in the future.

[1] G. K. Batchelor and A. A. Townsend, "Decay of vorticity in isotropic turbulence," Proc. R. Soc. London Ser. A **190**, 534 (1948).
[2] G. K. Batchelor and A. A. Townsend, "Decay of isotropic turbulence in the initial period," Proc. R. Soc. London Ser. A **193**, 539 (1948).
[3] G. K. Batchelor and A. A. Townsend, "Decay of turbulence in the final period," Proc. R. Soc. London Ser. A **194**, 527 (1948).
[4] Y. Sato and K. Yamamoto, "Empirical equations for the structure of isotropic turbulence," J. Chem. Eng. Jpn. **16**, 273 (1983).
[5] M. R. Smith, R. J. Donnelly, N. Goldenfeld, and W. F. Vinen, "Decay of vorticity in homogeneous turbulence," Phys. Rev. Lett. **71**, 2583 (1993).
[6] N. N. Mansour and A. A. Wray, "Decay of isotropic turbulence at low reynolds number," Phys. Fluids **6**, 808 (1994).
[7] J. R. Herring and R. M. Kerr, "Comparison of direct numerical simulations with predictions of two-point closures for isotropic turbulence convecting a passive scalar," J. Fluid Mech. **118**, 205 (1982).
[8] Th. von Kármán and L. Howarth, "On the statistical theory of isotropic turbulence," Proc. R. Soc. London Ser. A **164**, 192 (1938).
[9] C. G. Speziale and P. S. Bernard, "The energy decay in self-preserving isotropic turbulence revisited," J. Fluid Mech. **241**, 645 (1992).
[10] G. K. Batchelor, "Energy decay and self-preserving correlation functions in isotropic turbulence," Q. of Appl. Math. **6**, 97 (1948).
[11] L. G. Loitsianskii, NACA Tech. Memo. No. 1079, 1945.
[12] P. G. Saffman, "The large-scale structure of homogeneous turbulence," J. Fluid Mech. **27**, 581 (1967).
[13] J. O. Hinze, *Turbulence* (McGraw-Hill, New York, 1975).
[14] G. K. Batchelor and I. Proudman, "The large-scale structure of homogeneous turbulence," Proc. R. Soc. London Ser. A **248**, 369 (1956).
[15] L. F. G. Simmons and C. Salter, "Experimental investigation and analysis of the velocity variation in turbulent flow," Proc. R. Soc. London Ser. A **145**, 212 (1934).
[16] A. L. Kistler and T. Vrebalovich, "Grid turbulence at large Reynolds numbers," J. Fluid Mech. **26**, 37 (1966).
[17] G. Comte-Bellot and S. Corrsin, "The use of a contraction to improve the isotropy of grid-generated turbulence," J. Fluid Mech. **25**, 657 (1966).
[18] W. K. George, "The decay of homogeneous isotropic turbulence," Phys. Fluids A **4**, 1492 (1992).
[19] G. J. Barenblatt and A. A. Gavrilov, "On the theory of self-similar degeneracy of homogeneous isotropic turbulence," Sov. Phys. JETP **38**, 399 (1974).
[20] G. J. Barenblatt, *Similarity, Self-Similarity, and Intermediate Asymptotics* (Plenum, New York, 1979).
[21] S. A. Orszag, "Numerical simulation of incompressible flows within simple boundaries. i. galerkin (spectral) representations," Stud. Appl. Math. **L**, 293 (1971).
[22] R. S. Rogallo, "Numerical experiments of homogeneous turbulence," NASA Tech. Memo. No. 81315, 1981.
[23] P. K. Yeung and S. B. Pope, "An algorithm for tracking fluid particles in numerical simulations of homogeneous turbulence," J. Comput. Phys. **79**, 373 (1988).